Effect of damping components having slotted-structures on the instability induced by sliding friction

X. D. Lu[a,b,#], R. L. Wang[a,b,#], J. L. Mo[a,b,*], H. Ouyang[c,*] , Z. Y. Fan[a,b], Y. F. Zhang[d], J. Zhao[a]

[a] Tribology Research Institute, School of Mechanical Engineering, Southwest Jiaotong University, Chengdu 610031, China

[b] Technology and Equipment of Rail Transit Operation and Maintenance Key Laboratory of Sichuan Province, Chengdu 610031, China

[c] School of Engineering, University of Liverpool, Liverpool L69 3GH, UK

[d] Key Laboratory of Testing Technology for Manufacturing Process, Southwest University of Science and Technology, Mianyang, 621000, China

* Corresponding author: J.L. Mo

Tel.: +86 28 8760 0601; fax: +86 28 8760 3142.

E-mail address: jlmo@swjtu.cn

Abstract:

Experimental tests and numerical simulations are performed to explore the influence of damping components with slotted surface structures into a friction system on the dynamical instability. The damping components with slots at different depths are designed, combined with a special tribological test apparatus to evaluate their ability to stabilize the friction system. The experimental results show that slotted-structured damping components can dramatically reduce the vibration response of the system and the energy level at the dominant frequency, thus stabilizing the friction system. Specifically, the system containing shallow slots on the leading edge than that of the trailing edge can eliminate the tangential partial wear and show the greatest potential on reducing the unstable vibration. It can be further verified by finite element analysis. Moreover, it is found that the contact inclination angle between the disc and the pad plays an important role on the generation of instability of the system, which can be further explained through a two DOF-model with a contact inclination angle.

Keywords: Friction-induced vibration; Damping; Slotted-structure; Instability; Numerical.

#: These authors contributed equally to this study.

1. Introduction

Sliding friction is a considerably common physical concern in most mechanical systems and everyday life. Friction occurs in the joints of robots, meshing of gears in power transmission systems, between the disc and the pad in brakes, between the shoes and the ground when people walk, and other situations involving moving parts in contact [1-5]. Sliding friction often generates vibration at the contact interface, referred to as friction-induced vibration [6-8]. This vibration can lead to instability of the friction systems and emission of noise, consequently harming the mechanical equipment and the surrounding environment. This occurrence leads to fatigue damage of mechanical structures, excessive wear and failure of machine parts, and hearing damage. These adverse effects arising from instability of the systems can substantially shorten the service life of machine parts, and severely affect productivity and safety [9-11]. Therefore, the excitation of the instability of the systems needs to be elucidated and an improved approach to reducing instability is valuable.

Numerous studies using experimental tests, theoretical analysis, and the finite element method have thus far been conducted on the mechanism that allows friction-induced vibration to cause instability [12-15]. Factors affecting the instability of friction-induced vibration vary and involve complexity, such as loading conditions, material properties of the friction pair, contact interface characteristics, and damping and stiffness, among others [9, 16-18]. Several classical theories have also been proposed, aiming to explain the progress by which friction-induced vibration leads to instability. These mechanisms include for instance, stick-slip, Negative Friction-Velocity Slope and Mode lock-in.

As increasing interest is directed toward instability induced by sliding friction and its harm, various approaches to suppressing friction-induced unstable vibration have been proposed in recent decades. These approaches can be broadly classified as “direct” , where vibration energy is reduced at its source, and “indirect” , where vibration propagation is impeded [19-21]. At present, many studies believe that the unstable vibration of contact interface leads to the friction induced vibration. The typical direct method is to modify the contact interface, by introducing the slotted-structures and changing the brake materials [22, 23]. Lin et al. predicted the instability of a brake system, including various disc modifications by complex eigenvalue analysis, suggesting that relevant modification of the disc surface could greatly reduce instability and brake noise [24]. Oberst and

Lai evaluated numerically the effect of cutting a slot on the pad surface on the instability propensity using acoustic power calculation. They pointed out that a single vertical slot achieved the highest potential for suppressing unstable vibration [25]. Moreover, Kim et al. used a pad-on-disc apparatus to examine the friction-induced vibration characteristics of different automotive brake friction disc materials [26]. Gweon et al. demonstrated that the short glass fibre dispersion in brake friction materials significantly influenced friction instability of brake applications; the friction material with chopped glass fibres performed much better than that with milled glass fibres in reducing the unstable vibration [27]. Ahmed et al. indicated that the coated and non-coated discs markedly varied in instability generation; the coated disc particularly generated a weaker vibration [28].

Many other scholars believe that the friction induced vibration is due to the fact that the energy transmitted by the friction is greater than the energy dissipated during the friction process [29, 30]. Damping components are widely used in friction systems to reduce vibration because of their excellent energy dissipation ability. Damping components (damping shim) do not directly contact with friction contact interface, which is an indirect method to reduce the instability of the system. Nakra demonstrated the effect of unconstrained and constrained viscoelastic damping treatments on vibration control [31]. Triches Jr et al. found that the system could be stabilized by using the constrained layer damping integrated into the disc brake system to reduce vibration at resonance and dissipate the energy of the system [32]. Wang demonstrated that a slotted rubber block was capable of reducing the highest contact pressure concentration at the pad surface, thereby suppressing stick-slip oscillation [33]. Kang numerically examined the relationship between the in-plane modes of the disc and damping shims by using the finite element method, indicating that the damping shims could suppress the excitation of in-plane modes and reduce the propensity of the associated instability [34].

Our previous studies showed that the slotted damping components perform even better in stabilizing the friction system. It was found that the angle of the structure and the number of the slots can significantly affect the unstable vibration [35, 36]. However, the design criteria of the damping component are still not comprehensive, which requires further exploration. Therefore, damping components with slots of different depth is introduced to the friction systems to investigate the influence of slot depth on the instability of friction systems, and the relationship between

damping components and friction and wear on the contact surface is established. The research results can be learnt to design damping components with excellent performance in stabilizing friction systems, which has certain practical values.

In the current study, the dynamic instability phenomenon of a self-developed tribological test apparatus is studied in which damping components with different structures are introduced. Damping components having slots in different depths are designed, and their potentials to reduce vibration and modify the friction interface are evaluated. An experimental study on their instability of the system from the perspectives of dynamics and tribology simultaneously is performed. Subsequently, a simple finite element model is established to support the existence of contact inclination angle during sliding. Finally, a two-DOF model with contact inclination angle is proposed to verify the experimental occurrences.

2. Experimental description

2.1 Details of the test apparatus

To evaluate the abilities of different damping components in the vibration reduction, a special tribological test apparatus is developed to simultaneously acquire force and vibration acceleration signals. Fig. 1 presents a schematic of the test apparatus, which mainly consists of a tribological testing subsystem, a driving subsystem, and signal acquisition and analysis subsystems. A disc sample driven by a 3 kW AC servo motor rotates at a constant speed. A pad sample is mounted on the fixture which connects the 2-D force sensor and the axle. The measurement ranges of the force sensor from 0-2500 N, and the resolution is 1‰ F·S. In the initial stages of the test, the cylinder pushes the axle to together with the connector and the 2-D force sensor downloaded, then to make the pad sample rub the rotating disc sample, generating sliding friction at the contact interface between the two components. The 3-D acceleration sensor is mounted in front of the fixture with the following parameters, measurement range up to 125 g, frequency range, 0.5 Hz to 7 kHz, sensitivity, 42 mV/g, and mass, 13 g. These sensors are connected to a 16-channel data acquisition instrument. The coordinate system is established. The x-direction and y-direction are tangential direction and normal direction, respectively. Additional details on this test apparatus are provided in our previous study [36].

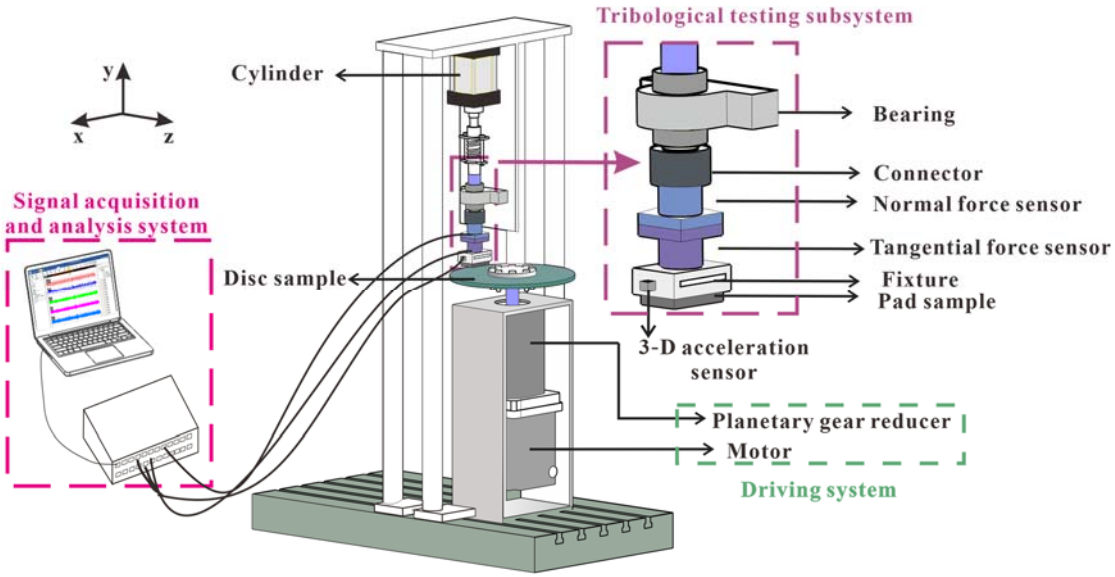

Fig. 1 Schematic of the test apparatus

2.2 Experimental samples

The sample pad is mainly prepared by hot pressing of a copper-based powder metallurgy composite. The pad sample has a height of 20 mm and is a rectangular area of 60 mm×40 mm. This rectangular area is the apparent contact area of the friction pairs. The disc sample is made from Q345 steel, whose dimension parameters are an external diameter, 316 mm, an internal diameter, 80 mm, and a thickness, 15 mm.

Cutting the slots on the one of contact surface of damping components is a relatively simple and convenient method to better suppress friction-induced vibration, and each at a different depth is investigated their ability to reduce vibration. The damping component are inserted between the fixture and the pad, with the slotted surface in close contact with the back plate of the pad, as shown in Fig. 2 (a). With its design based on the shape of the pad sample, the damping component has a height of 5 mm and a rectangular area of 60 mm × 40 mm, and is made from Styrene Butadiene Rubber (SBR). The reason for selecting SBR as the damping material is that it is the most common vibration isolation components for various structures. Figs. 2 (b) and 3 present schematic views of damping components with parallel slots in different depths. The geometric parameters of the damping components are listed in Table 1.

To conveniently distinguish damping components without slot and with slot depths of 1-mm, 2-mm and 3-mm (Fig. 2 (b)), the components are designated as D0, and D1, D2 and D3. The corresponding friction system is referred to as the D0, D1, D2, and D3 system. In addition, in order

to further study the effect of slots with different depths on the instability of the systems, three additional damping components, each having slots in two different depths of 1 mm and 3 mm are fabricated, D-1-3, D-3-1 and D-C, as shown in Fig. 3. Corresponding friction systems are also defined as previously described, such as the D-1-3 system. The purpose of having three specifically slotted damping components is clarified in Section 3.1.3.

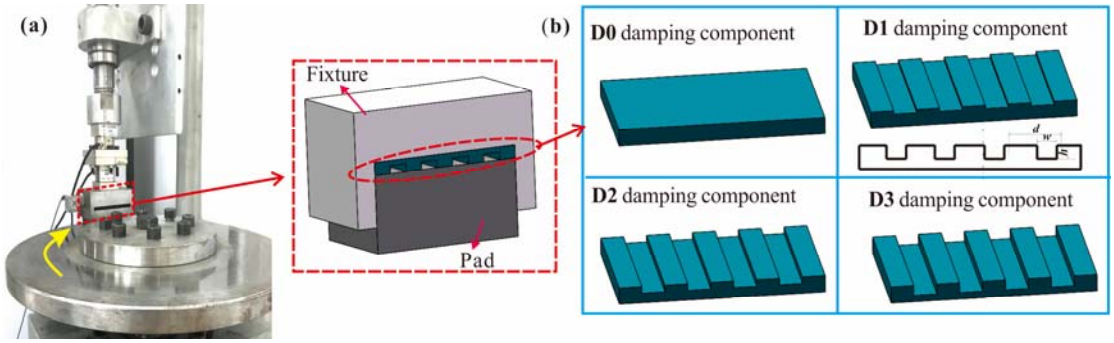

Fig. 2 Mounting location of the damping components (a) and structural drawing of the damping components (b)

Table 1 Geometric parameters of the damping components

Damping components	Pitch *d* (mm)	Width *w* (mm)	Depth *h1* (mm)	Depth *h2* (mm)
D0	13.3±0.2	6.7±0.2	/	/
D1	13.3±0.2	6.7±0.2	1±0.2	/
D2	13.3±0.2	6.7±0.2	2±0.2	/
D3	13.3±0.2	6.7±0.2	3±0.2	/
D-1-3/ D-3-1/ D-C	13.3±0.2	6.7±0.2	1±0.2	3±0.2

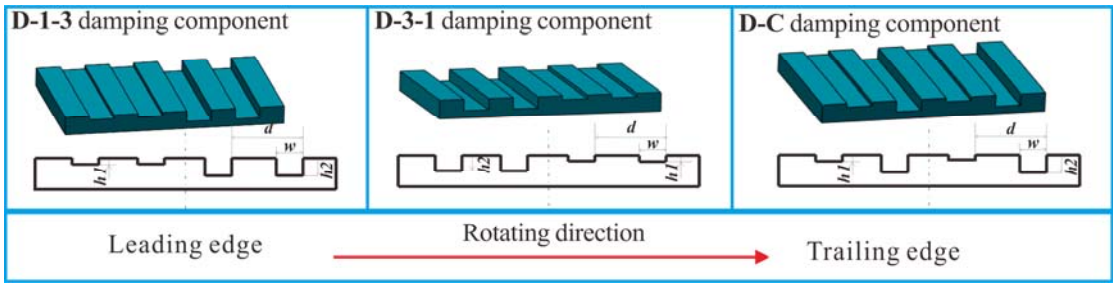

Fig. 3 Structural schematic view and the mounting location of two different depth slots of the damping components

2.3 Experimental preparation

Before formal tests are conducted, several pre-tests are performed under different normal loads

and disc rotation speeds. When the speed is selected as 25 rpm and the constant load is 500 N by pre-tests, the friction system (Original system) without damping component generates considerably strong vibration. Therefore, the following formal tests are performed under those same parameters to evaluate the abilities of damping components of different structures to reduce the vibration. All signals acquired by sensors are set to a sampling rate of 10000 Hz.

In this work, each test is performed not less than four times to ensure good reliability and repeatability of the experimental results. At the start of each test, all contact surfaces of the disc and the pad samples are cleaned with alcohol and then dried by blowing air. Each test is conducted at intervals of 20 min to dissipate heat generated from friction. The experimental environment of all tests in this study is strictly controlled that the ambient humidity is 60%±10% RH, and the temperature is 24□~27□. After each test, the wear morphology of the pad sample is observed using a Bruker Contour GT white light interferometer.

3. Results and discussions

3.1 Experimental results and analysis

3.1.1 Analysis vibration characteristics

To evaluate the performance of the damping components having slots with different depths in reducing the vibration, normal and tangential vibration acceleration signals of each friction systems acquired using the 3-D acceleration sensor are analyzed (Fig. 4). Time histories while testing from 50 s to 80 s are shown, that is, the period during which signals have become steady. For the Original system, visible oscillation and large amplitude of acceleration signals are observed in both normal and tangential directions, indicating that vibration induced friction is generated during sliding. For the damping systems, the vibration amplitude shown in the time-domain is significantly reduced, and oscillation fluctuation also decreases, suggesting that the damping components are conductive to reduce the unstable vibration of the friction system. Further comparison of the vibration accelerations of the systems having the damping components with slots in different depths indicates lower vibration amplitudes and considerably weak oscillation for the D2 system.

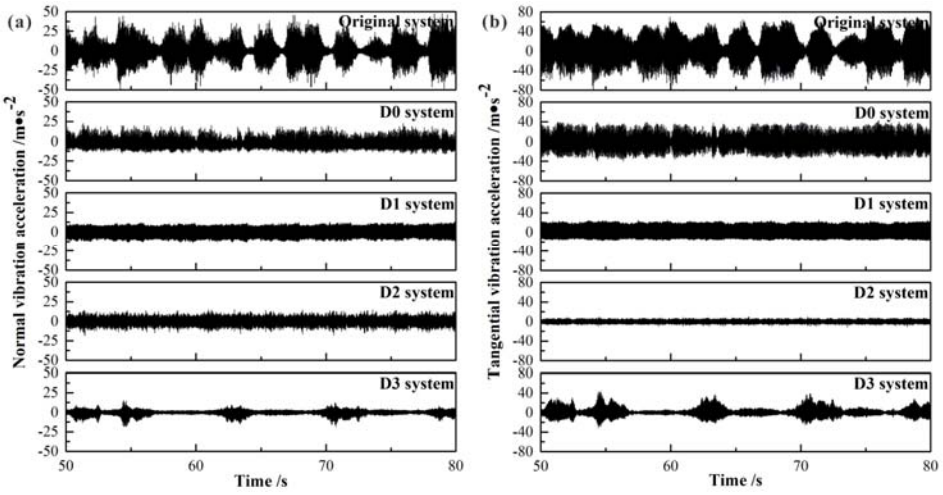

Fig. 4 Time history records of normal (a) and tangential (b) vibration accelerations for different systems

$$\mathrm{RMS}=\sqrt{\frac{a_1^2+a_2^2+\cdots+a_n^2}{n}} \tag{1}$$

The root-mean-square (RMS) values of normal and tangential vibration accelerations from 50 to 80s are selected and calculated to intuitively compare the ability of different damping components to suppress unstable vibration. The calculating formula of the RMS is shown in equation (1), where a_i represents the amplitude of the i-th point collected by the acceleration sensor, and n represents the data length. The results are presented in Fig. 5. The RMS values of the Original systems is markedly great than those of the other four systems. Specifically, D2 system shows the minimum RMS values in both normal and tangential directions. Therefore, introducing the damping components can help to reduce the vibration response of the friction system, and the damping components with slots at different depths, such as the D2 damping component, exhibit increased potential for suppressing vibration.

Modal tests are performed to obtain the natural frequency of the system. The disc is at a stationary state, on which a 500 N normal force is applied through the cylinder. Then we strike the fixture in the friction direction using a hammer. The modal test result shows a natural frequency of 67.1 Hz.

Moreover, power spectrum density analysis (PSD) of vibration acceleration in the tangential direction is performed to study the of vibrational energy distribution of the systems in the frequency domain. As shown in Fig. 6, the energy of the Original system is mainly concentrated at the

dominant frequency of 61.0 Hz and a series of harmonics. One can note that there is a slight difference between the dominant frequency of the system having the damping components and that of that the Original system. Considering a fact that the natural frequencies of the friction system is strongly related to the system structures and the materials properties, and the relatively small and soft damping components have little effect in affecting the system structures and materials properties, thus the fundamental vibration frequency of the friction system may not change significantly. The power spectral density of the of vibration acceleration in the tangential direction shows that the dominant frequencies of the Original system and the D0 system are 61.0 Hz and 64.6 Hz, respectively, while the dominant frequency of the three damped systems is 67.1 Hz. The small difference between the Original system and the damped system may be caused by the introduction of damping components having different slotted-structures. In addition, the friction systems with damping components have obviously less excited high frequency vibration and can reduce the energy intensity of the dominant frequency. By contrast, for the D2 system, no dominant frequency in the entire frequency range is observed; weak vibration is acquired throughout the test. These results indicate that adding an appropriate damping component into the system can reduce the energy at the dominant frequency and the contributions from other frequencies, thus stabilizing the friction system. This natural mode is very close to the dominant frequency of the experimental result; It can be considered that the dominant frequency of the acceleration vibration originates from this natural mode of the friction system.

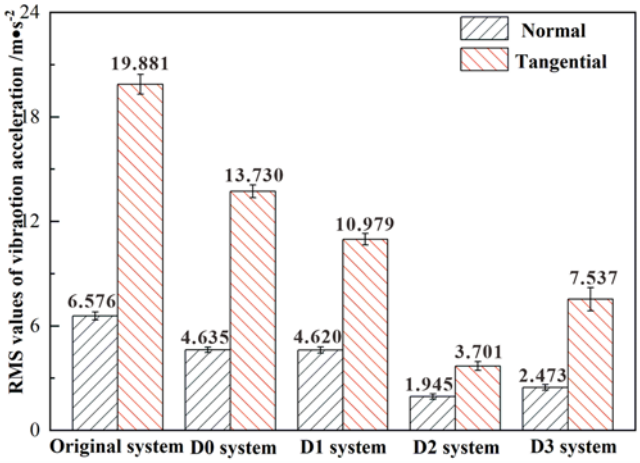

Fig. 5 RMS values of vibration accelerations in both normal and tangential directions

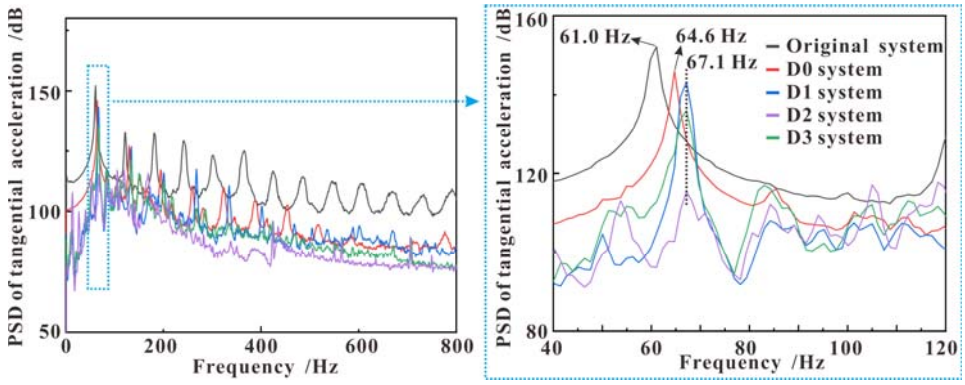

Fig. 6 Power spectrum density analysis of tangential vibration acceleration for different systems

3.1.2 Friction and wear analysis

From the tribological perspective, the influence of damping elements on the vibration response of the system is discussed from the view of interface wear, and the friction wear of different friction systems is analyzed. Fig. 7 presents the friction coefficient curves for the testing duration of 50-80 s. The black fine line represents the actual friction coefficient, which is the ratio of the friction forces to normal forces measured using the 2-D force sensors. In order to better compare the fluctuation trend of different systems, the red thick line obtained by smoothing to filter the high-frequency and random signals of actual friction coefficient represents the average friction curve. The Original system and D0 system have the larger fluctuation of friction coefficient among these five systems. The D2 system has a larger average friction coefficient value than those of the other four systems. Moreover, it is worthwhile noting that the fluctuation of the actual friction coefficient for D1 and D3 system is obviously larger than that D2 system. These findings combined with the vibration response characteristics of the systems, suggest that a larger fluctuation in the friction coefficient reflects a greater system instability.

The interface characteristics of a worn surface highly correlate with the vibration response of the systems [38, 39]. Our previous works indicated that the degree of wear on the sides of the leading edge and the trailing edge on a pad surface was significantly different, which could influence the vibration characteristics of the system [36]. Thus, surface topography analysis is conducted in the current study. Wear topography analysis is also performed to establish the relationship between the contact interfacial characteristics of the friction pairs and the dynamic response characteristics of the system, as well as to determine the process by which damping components influence contact at

the interface and correspondingly change the vibration of the system.

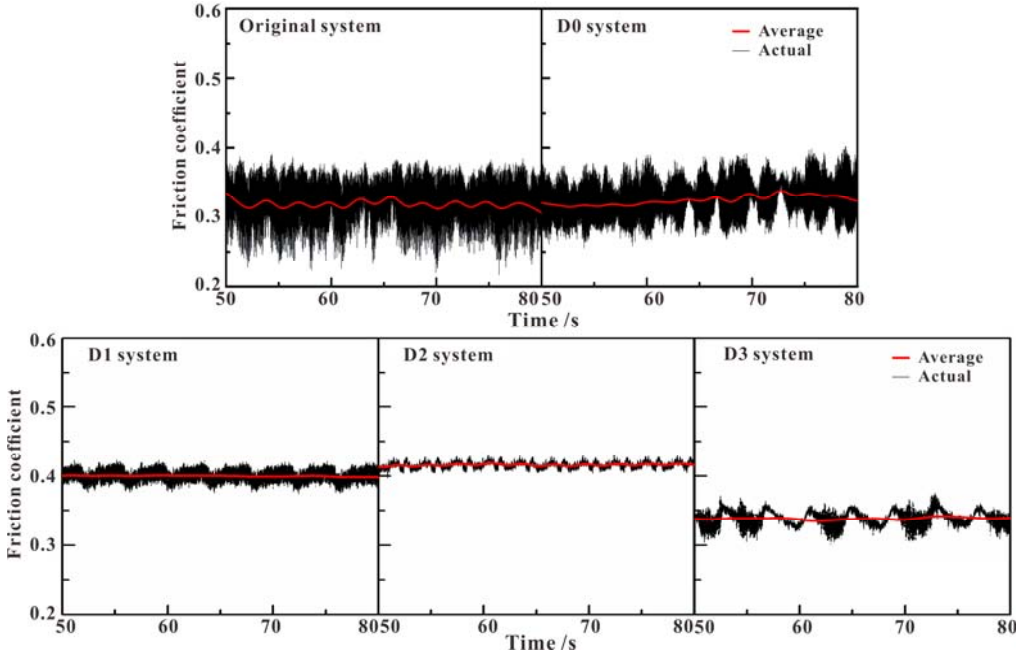

Fig. 7 Friction coefficient curves for the period time of 50-80 s

The surface morphologies of the friction pads of slot damping systems are obtained after the test, as shown in Fig. 8. The wear behavior of the three pad surfaces shows a trend similar to that of a worn surface with the leading edge being smoother than the trailing edge, which results from constant rubbing between the leading edge of the pad and the disc. The microscopic wear of different areas on the pad surface is examined using three-dimensional topographies for the D2 system to verify the wear difference between the leading and trailing edges of the pad. The results show that the worn surface of the side of the leading edge is flat and smooth, whereas the other side is rough, with an accumulation of scattering wear debris. These occurrences indicate that a contact inclination angle exists between the disc and the pad friction pair during sliding, as shown in Fig. 9. With the difference in wear between the leading and trailing edges considered, the contact inclination angle can reflect the tangential partial wear of the pad surface to a certain extent. Therefore, among the three systems, the D1 system has the smallest wear area with the most severe partial wear, which corresponds to the largest contact inclination angle. By contrast, the D2 system has the largest wear area, which corresponds to the smallest contact inclination angle.

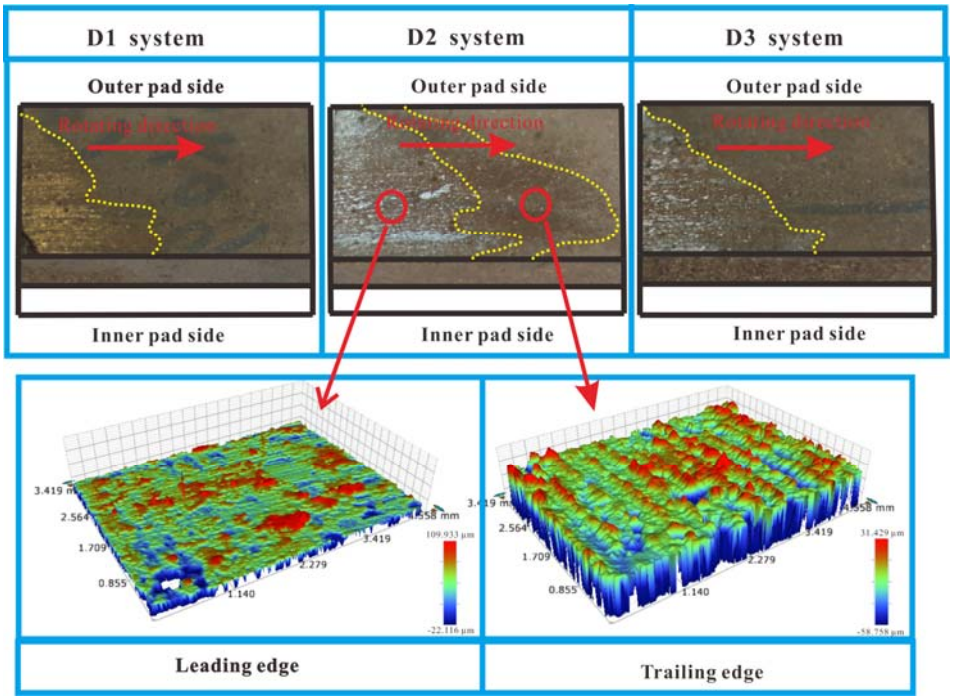

Fig. 8 Surface topographies of the pad surfaces of the three friction systems after the test

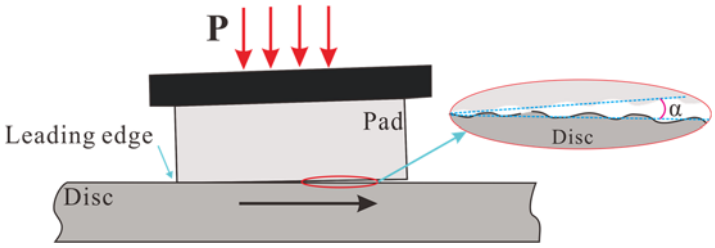

Fig. 9 Schematic of the contact inclination angle between the friction pair

On the basis of the aforementioned vibration characteristics, the D1 system has the larger vibration and severe tangential partial wear of the pad surface, whereas the D2 system exhibits the opposite results. Therefore, the dynamic response of the system is highly correlated with the contact inclination angle. The friction systems with the slotted damping components are speculated to change the contact inclination angle during sliding. Consequently, the contact status at friction interface is improved, thereby the unstable vibration of the system is reduced.

3.1.3 Further validation the influence of slot depth of damping components on vibration and tribological characteristics

Compared with the friction system having the smooth damping component, that with slotted damping component can reduce the vibration of the system to varying degrees, as revealed in the aforementioned experiments. The slot depth of the damping components can affect their overall deformation so as to adjust the contact angle between the pad and the disc, and finally affect the

vibration of the system. To further verify this conjecture, a damping component with slots in two different depths is introduced to amplify or reduce the deformation of the damping component. The aim is to amplify the influence of the contact inclination angle between the pad and the disc on the vibration of the friction systems. Three special slotted-damping components are thus evaluated (Fig. 3 presents the detailed structural parameters of the three damping components).

Fig. 10 shows the time history records of the vibration acceleration of the systems using the three special slotted damping components. For the D-1-3 system with a damping component that has a slot at a depth of 1 mm on the side of the leading edge and 3 mm on the side of the trailing edge of the pad surface, the vibration acceleration amplitude always stays at a lower level, and no obvious fluctuation occurs. By contrast, for the D-3-1 system, the vibration acceleration largely fluctuates, and the vibration amplitudes are large. For the D-C system, the vibration ranges between that of the D-3-1 and D-1-3 systems. The RMS values of the vibration acceleration in normal direction and tangential direction can reveal the difference in vibration intensity among the three systems, as shown in Fig. 11. The D-1-3 system exhibits the weakest vibration, whereas the D-3-1 system shows the strongest vibration. These results indicate that the D-1-3 system with damping component can reduce the system instability, while the D-3-1 damping component not be helpful. It's worth noting that the RMS values of the tangential and normal vibration acceleration of the D-1-3 system are also less than that of the D2 system, which indicates that D-1-3 damping components can better reduce the vibration amplitude of the friction system.

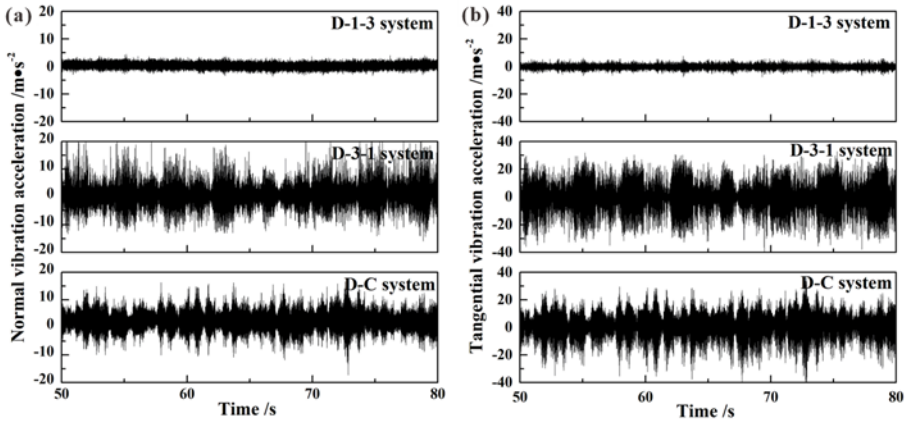

Fig. 10 Time history records of normal (a) and tangential (b) vibration accelerations for different systems

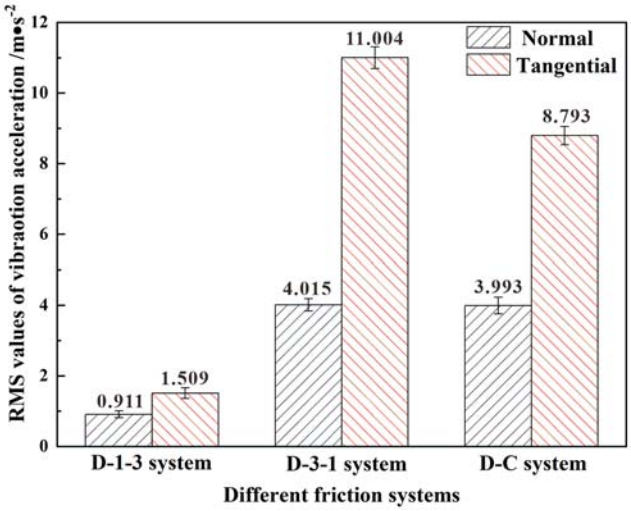

Fig. 11 RMS values of vibration accelerations in both normal and tangential directions

The Fourier transform of the tangential vibration acceleration signal directly collected by the data acquisition instrument is performed to obtain the power spectral density analysis results, as shown in Figure 12. In order to more directly compare the influence of without damping components, a damping component having constant slot depth or a varying slot depth on the dominant frequency of the vibration acceleration, the power spectral density analysis results of the Original system and D2 system are shown in Fig.12. The dominant frequencies of D-3-1 system and D-C system are slightly different from that of the Original system, and the energy intensity of the dominant frequency of D-3-1 system and D-C system has decreased compared with that of the Original system to a certain extent. For the D-1-3 system and D2 system, no dominant frequency is observed and the power density is reduced relative to other systems, indicating that the D-1-3 damping component and D2 damping component can well suppress the excitation of vibration and hence reduce the instability of vibration.

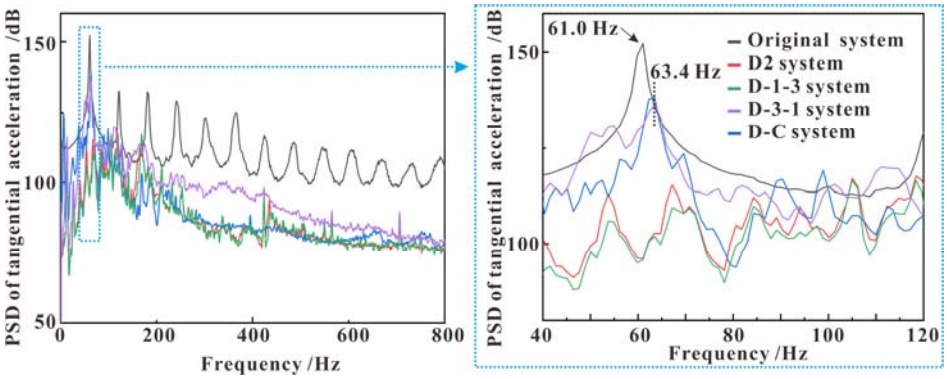

Fig. 12 Power spectrum density analysis of tangential vibration acceleration for different systems

Fig. 13 presents the friction coefficient curves of the system having the three special damping components, measured over a period of 50-80 s. The D-1-3 system has the largest average friction coefficient and the weakest vibration response. By contrast, the D-3-1 system and D-C system, which generate stronger vibration than that of the D-1-3 system, show more significant fluctuation of the actual friction coefficient. These experimental phenomena are consistent with those in Section 3.1.2.

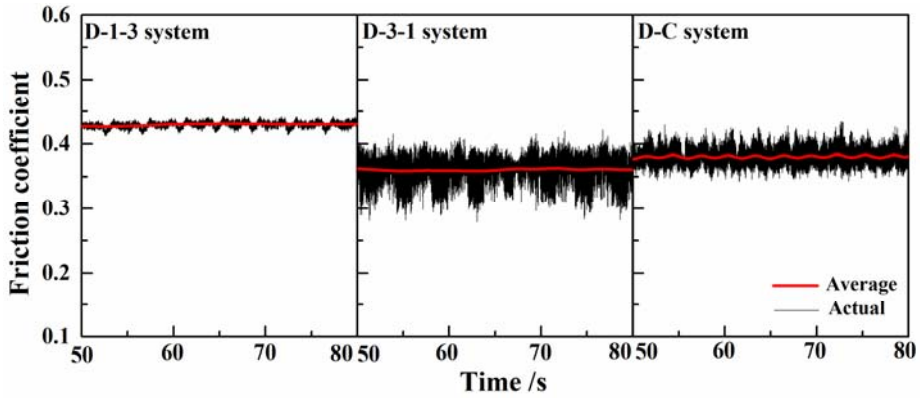

Fig. 13 Friction coefficient curves for the period time of 50-80 s

Fig. 14 presents the morphologies of worn surface of the pad in three systems having the special damping components. For the D-1-3 system, both the side of leading edge and that of the trailing edge on the pad surface exhibit wear track, indicating that tangential partial wear is nearly non-existent on the pad surface. For the D-3-1 system and D-C system, wear track is observed only on the leading edge on the pad surface, indicating that there is visible tangential partial wear. These observations suggest that the contact behavior of the friction pair in the D-1-3 system form a good fit, which corresponds to the minimal contact inclination angle.

The wear area on the pad surface is further analyzed using three-dimensional topographies. The D-3-1 system and the D-C system exhibit more complex wear morphologies showing visible ploughings and micro-slots and contact plateaus; meanwhile the D-1-3 system produces no serious wear at the contact interface. Therefore, introducing the D-1-3 damping component into the friction system can significantly improve the wear condition at the contact interface.

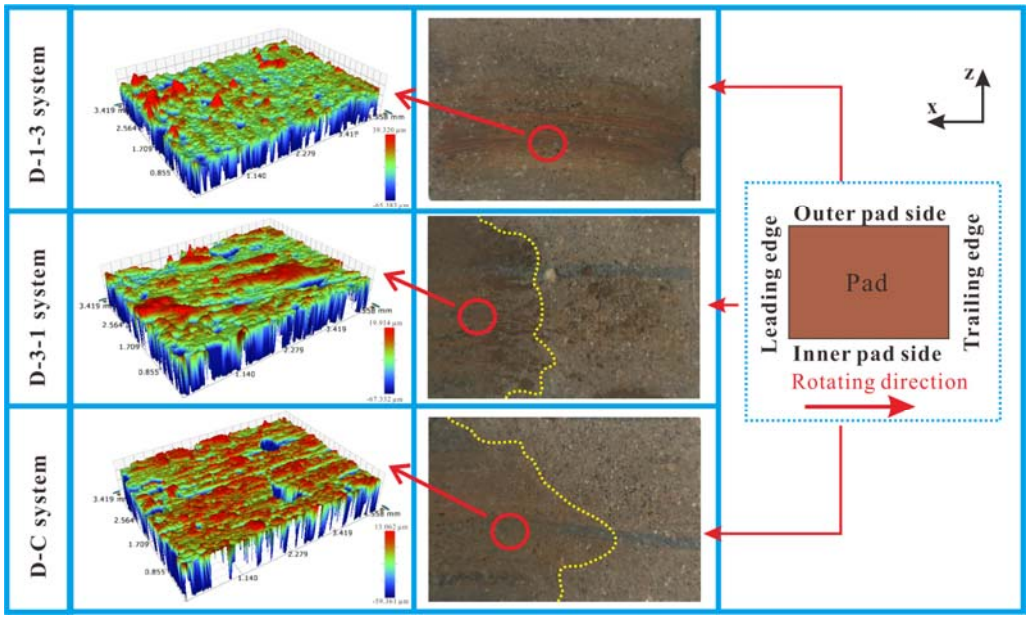

Fig. 14 Surface topographies of the pad surfaces of the three friction systems after the test

To further determine the effect of the contact inclination angle on the instability of the system, two-dimensional profiles at three locations on the pad surface along the tangential direction (rotating direction of the disc) are measured. The results are presented in Fig. 15. Lines 1, 2, and 3 represent the leading edge, center and trailing edge on the pad surface in the tangential direction, respectively. For the D-1-3 system, the two-dimensional morphologies at the three locations are similar (refer to the values of R_a), indicating that the pad surface is relatively uniform, and no tangential partial wear occurs. Meanwhile, the value of R_a at the leading edge of the D-3-1 and D-C system is significantly lower than that in the D-1-3 system, but the roughness of the trailing edge is similar to that of the unworn surface (R_a =0.976 for the unworn surface). This observation demonstrates that the leading edge increases smoothness owing to continuous rubbing. Meanwhile, the trailing edge on the pad hardly touches the disc. Moreover, the value of R_a is markedly larger at the pad center of the D-3-1 and D-C systems than that of the D-1-3 system, resulting in the accumulation of wear debris in large amounts. Therefore, the D-1-3 system has the smallest contact inclination angle between the friction pair.

With the vibration response of the system, and the friction and wear characteristics of the pad contact surface considered, it can be speculated that a larger the contact inclination angle indicates a more severe tangential partial wear and stronger vibration response for the corresponding friction system. Compared with the other systems, the D-1-3 damping component is found to have a better

performance in stabilizing the friction system.

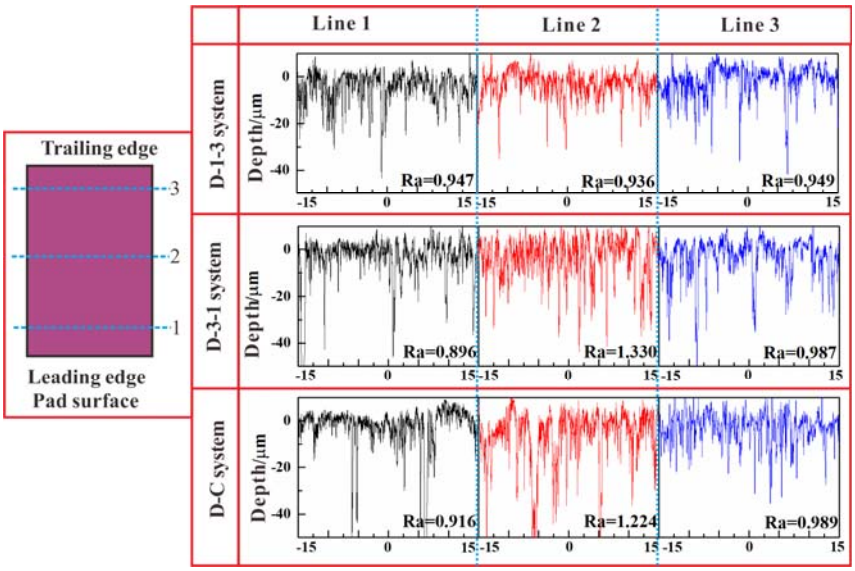

Fig. 15 Two-dimensional profile at three locations on the pad surface

3.2 Numerical simulation and result analysis

3.2.1 Creation of the finite element model

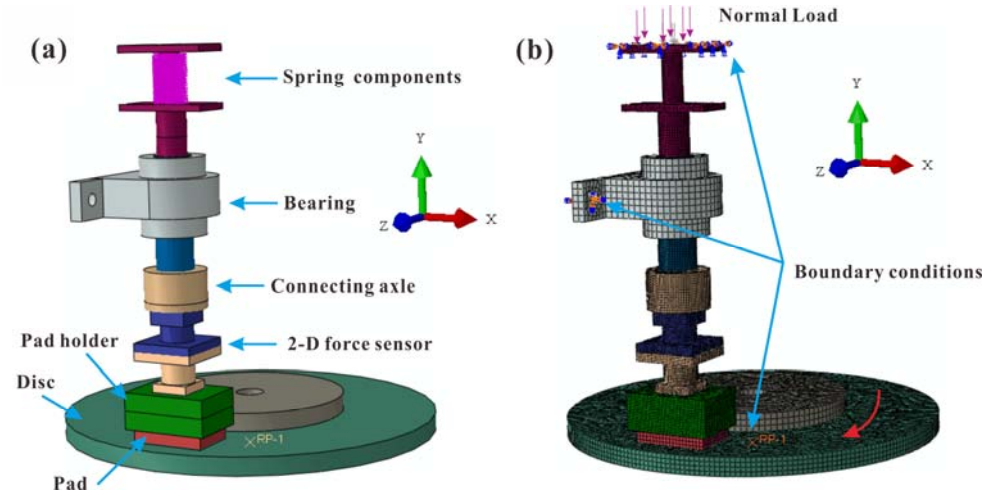

Fig. 16 The FE model of the test apparatus (a) and the corresponding load and boundary conditions (b)

The contact stress distribution on the pad surface and the deformation behavior of the pad in different friction systems are simulated using finite element software ABAQUS. First, a simplified finite element model is established based on experimental bench, which mainly consists of seven parts: a spring component, a bearing, a connecting axle, a 2-D force sensor, a pad holder, a disc, and a friction pad. The material properties of the components are provided in Table 2. The rubber material is defined as the hyperelastic material, which indicates that such kind of material is not

depended on the young's modulus and the poisson's ratio (these two parameters are used to reflect the material property of the linear elastic material). Therefore, the young's modulus of rubber material is not set in finite element model. The material properties of the other components have been fully marked in terms of density, Young's modulus and poisson's Ration. And the setting of parameters of the damping material usually has little effect on the results of the finite element analysis but significantly increases the calculation time. Therefore, the parameters of the damping material are not set in the finite element model. For friction pairs, the disc is defined as the master surface because of its harder material and coarser mesh, and the pad surface is accordingly set as the slave surface. Fig. 16 (b) shows the boundary conditions as well as the load of the finite element model set based on the actual conditions of the test bench. Friction-generated heat is excluded in this numerical analysis.

Table 2 Material properties of the components in the finite element model.

Part	Density/g/cm^3	Young's Modulus/GPa	Poisson's Ratio	Mooney-Rivlin Parameter
Backplate	7000	180	0.3	/
Pad	4000	20	0.24	/
Pad holder	7800	196	0.3	/
Spring Components	7800	196	0.3	/
Connecting axle	7800	196	0.3	/
Disc	7800	210	0.27	/
Bearing	7850	210	0.28	/
Damping Components	/	/	0.499	C10=0.36 C01=0.09

By establishing the finite model of the Original system, D2 system, D-1-3system, and D-3-1 system, the friction systems having damping components with slotted surface structures are proven to change the contact inclination angle between the pad and the disc in the sliding process. Fig. 17 (a) shows the contact stress distribution on the surface of different pads. Obviously, the overall contact pressure of D-1-3 system is the lowest, and the distribution area of contact pressure is the widest. To more accurately observe the deformation of the pad, the sloping path on the pad surface with 7 nodes is selected as denoted by a dotted line in Fig. 17(a), to obtain the normal deformation displacement of the pad. The deformation along the oblique line can more accurately represent the deformation of the whole pad surface. Due to the reason of grid division, 7 nodes are selected to

form an oblique broken line that is almost the same as an oblique line. The deformation mainly occurs at the leading edge and slightly at the trailing edge resulting in the contact inclination angle. The Original system has the largest difference in the deformation between the leading edge and the trailing edge; thus, it has the largest contact inclination angle, which is in contrast to the contact inclination angle of the D-1-3 system, which is the smallest. The contact inclination angles of the D-3-1 system and D2 system are in the middle. These findings are consistent with the experimental results. The D-1-3 damping component has a better performance in stabilizing the friction system. Owing to the uneven contact pressure distribution on the pad contact interface during sliding friction, the deformation of the leading edge varies from that of the trailing edge on the pad surface, which leads to the formation of a contact inclination angle between the pad and the disc. Moreover, the slotted-structured damping components can change the contact angle between the pad and the disc in the friction system.

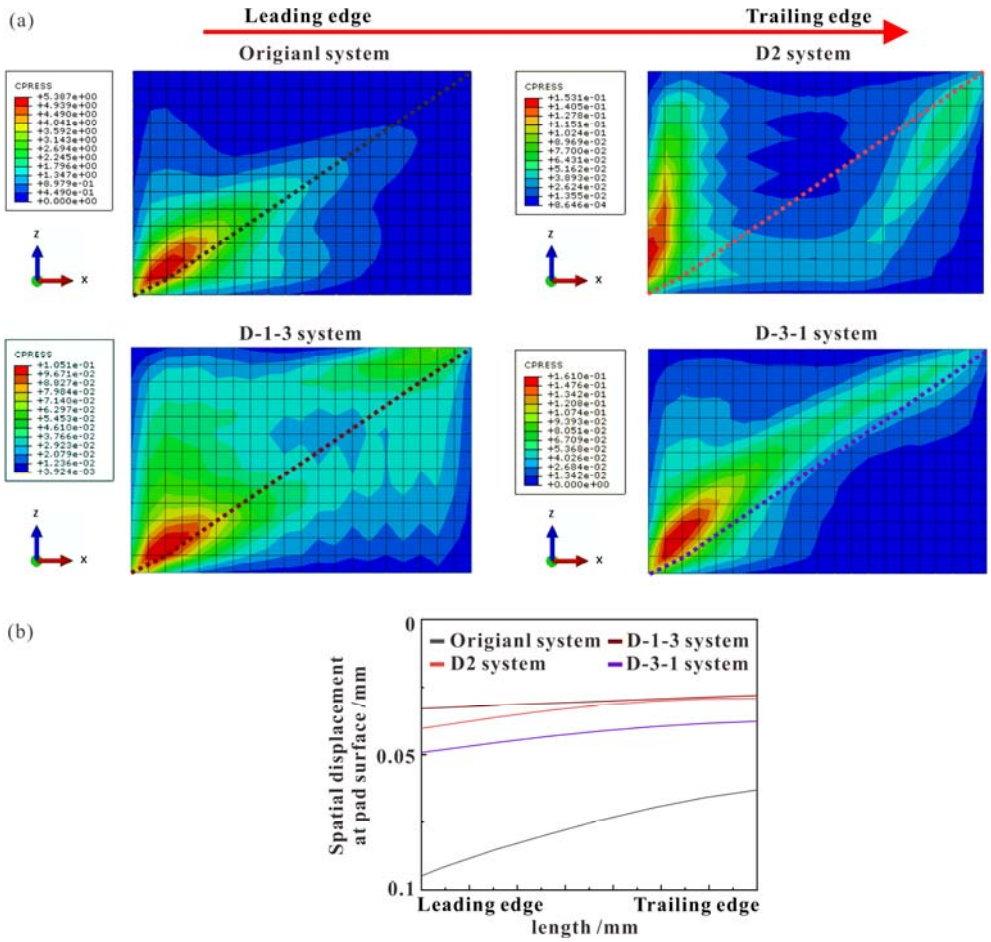

Fig. 17 Contact pressure distribution on the pad surface (a) and the deformation of the pad in oblique broken direction (b) for different friction systems

3.2.2 Contact inclination angle

As a matter of fact, the reason why the eight friction systems perform so differently lies in the different interfacial contact inclinations angle. To examine the influence of the contact inclination angle between the disc and the pad on the instability of the system, the numerical model considering the partial wear is developed based on a minimal single mass two-DOF model presented by Hoffmann et al. [40], in which the tangential partial wear is reflected by the contact inclination angle α (Fig. 18). It should be noted that the model is intended to illustrate the mode-coupling instability caused by the contact inclination angle instead of predicting the role of the slots on the damping components in determining the dynamical response of the friction system. Therefore, there is no need to consider the geometry of the damping components. Meanwhile, note that these parameters used in this numerical model is for the sake of calculation convenience, which do not represent the real parameters of the test rig. Therefore, the numerical model is only able to explain the experimental phenomenon, i.e., a large contact inclination angle tends to aggravate the instability of the friction system. However, it cannot give any substantial predictions to the real friction system. This model consists of a mass block and a rigid conveyor belt moving at a constant velocity. The mass block has an inclination angle in the tangential direction, simulating the contact inclination angle during the experimental tests. The mass block is supported by linear springs k_1 and k, spring k installed at an inclination angle of 45 ° and two viscous dampers, c_1 and c_2. Spring k_1 and viscous c_1 are the horizontal constraints on the mass block, similarly, spring k_2 and viscous c_2 are the normal constrain. The coupling between tangential direction and normal direction of the model is established by introducing spring k. Spring k_n connects the mass block with the rigid belt, representing the contact between the pad sample and the disc sample in the real test rig. The x-direction and y-direction shown in the Fig. 18 are denoted as tangential and normal directions respectively. For the tangential direction, a constant friction coefficient μ is assumed, and the classical Coulomb's friction law $F_f=\mu k_n y$ is used. This study aims to evaluate the effects of different contact inclinations angles on the instability of the systems. Other parameters of this system are set as following: m = 1 kg, k_1 = 7.017 N/m, k_2=2, k = 2.49 N/m, k_n = 5 N/m, and c_1 = c_2 = 0.02.

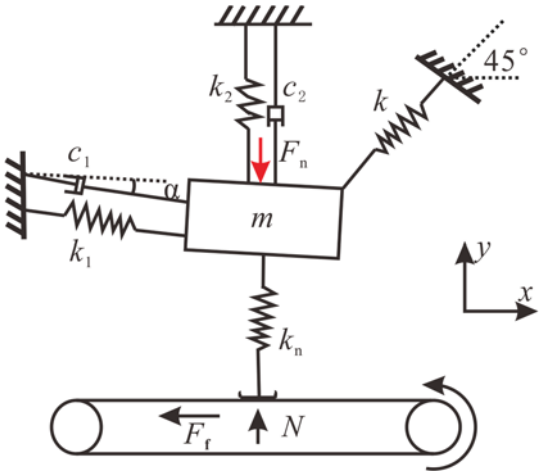

Fig. 18 The two-DOF numerical model with a contact inclination angle α

Assuming that the belt has no relative displacement in the normal direction, the motion equation of this model can be derived as follows:

$$\begin{aligned} &mx'' + c_1\cos^2\alpha x' - c_1\sin\alpha\cos\alpha y' + (k_1 cos^2\alpha + \frac{1}{2}k)x \\ &+(-k_1\cos\alpha\sin\alpha + \frac{1}{2}k)y = -F_f \\ &my'' + (c_2 + c_1\sin^2\alpha)y' - c_1\sin\alpha\cos\alpha x' + (-k_1\sin\alpha\cos\alpha + \frac{1}{2}k)x \\ &+(k_1\sin^2\alpha + \frac{1}{2}k + k_2 + k_n)y = -N \end{aligned} \tag{2}$$

Eq. (1) is rearranged thus:

$$\mathbf{Mx''+ Cx'+ Kx = 0} \tag{3}$$

where the damping matrix and the stiffness matrix can be obtained as:

$$\mathrm{C} = \begin{pmatrix} c_1\cos^2\alpha & -c_1\sin\alpha\cos\alpha \\ -c_1\sin\alpha\cos\alpha & c_2 + c_1\sin^2\alpha \end{pmatrix}$$

$$\mathrm{K} = \begin{pmatrix} k_1\cos^2\alpha + \frac{1}{2}k & -k_1\cos\alpha\sin\alpha + \frac{1}{2}k - \mu k_n \\ -k_1\sin\alpha\cos\alpha + \frac{1}{2}k & k_1\sin^2\alpha + \frac{1}{2}k + k_2 + k_n \end{pmatrix}$$

Complex eigenvalues analysis (CEA) is a highly efficient method for predicting the instability of the friction systems and thus is widely adopted in finite element analysis and numerical simulations [9, 12, 24]. The real parts of the eigenvalues of the equation of motion can generally reflect the stability of the system. The system is stable when all real parts of eigenvalues are negative, whereas the system becomes unstable when any real part of an eigenvalues is positive. The state

equations of Eq. (3) can be derived as

$$\begin{bmatrix} z_1' \\ z_2' \\ z_3' \\ z_4' \end{bmatrix} = \begin{bmatrix} 0 & 1 & 0 & 0 \\ \dfrac{-k_1\cos^2\alpha - \dfrac{1}{2}k}{m} & \dfrac{-c_1\cos^2\alpha}{m} & \dfrac{k_1\cos\alpha\sin\alpha - \dfrac{1}{2}k + \mu k_n}{m} & \dfrac{c_1\sin 2\alpha}{2m} \\ 0 & 0 & 0 & 1 \\ \dfrac{k_1\sin 2a}{2m} & \dfrac{c_1\sin 2\alpha}{2m} & \dfrac{-k_1\sin^2 a - \dfrac{1}{2}k - k_2 - k_n}{m} & \dfrac{-c_2 - c_1\sin^2 a}{m} \end{bmatrix} \begin{bmatrix} z_1 \\ z_2 \\ z_3 \\ z_4 \end{bmatrix}$$

In order to clarify the influence of the contact inclination angle on the mode-coupling instability, the results of the complex eigenvalue with the friction coefficient as the contact parameter are shown in Fig. 19. According to paper [41], frequencies cannot be perfectly merging due to the existence of the non-proportional damping in the model system (Fig. 19 (a)). In Fig. 19 (b), the friction coefficient when the real part of the eigenvalue changes from negative to positive is defined as the critical friction coefficient μ_c. When the contact inclination angle is 2.07°, the critical friction coefficient is 0.2.

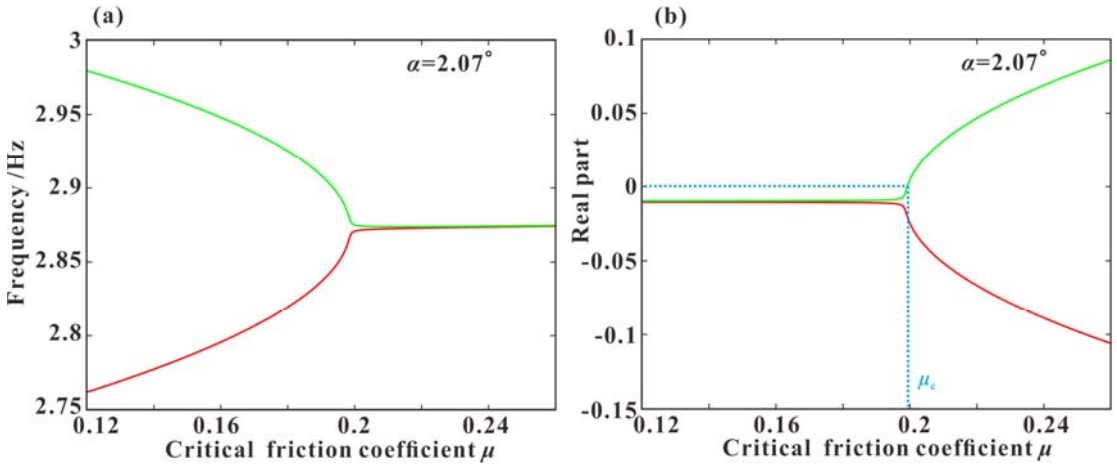

Fig. 19 Frequency (a) and real part (b) of the eigenvalue analysis of the two-DOF numerical model

The transient dynamic characteristics of this model are calculated using Runge-Kutta methods to estimate the effect of the contact inclination angle α on the instability of the system in the time-domain. The results are present in Fig. 20. Moreover, when critical friction coefficient μ_c = 0.2, a contact inclination angle α_c = 2.07 ° exists (Fig. 19). For $\alpha < \alpha_c$, the system produces steady periodic vibrations in both the tangential direction and normal direction, indicating that the system is stable. For $\alpha=\alpha_c$, the normal vibration amplitude increases linearly, and the tangential direction remains in

periodic motion, indicating a change in system stability from stable to unstable. As the contact inclination angle α further increases ($\alpha>\alpha_c$), both the tangential direction and normal direction vibration amplitudes increase exponentially with time, resulting in a more violent vibration in the system than that in the other two cases. The results show that the contact inclination angle will lead to the modal coupling and cause more unstable vibration of the friction system.

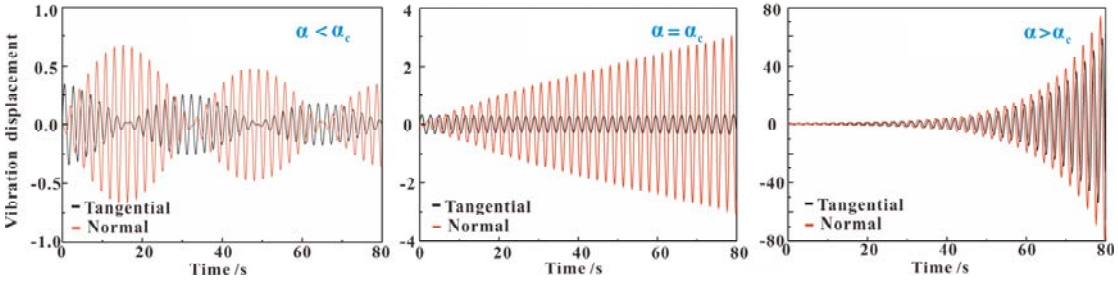

Fig. 20 Tangential and normal vibration displacements of the two-DOF numerical model for different inclination angles

In order to obtain the instability area of the system under the influence of the contact inclination angle, the critical friction coefficient corresponding to different contact inclination angle is obtained through complex eigenvalue analysis. The results are shown in Fig. 21. The critical friction coefficient decreases with the increase of the contact inclination angle. When the contact inclination angle α increases, the region of instability increases, which indicates that the system is prone to instability.

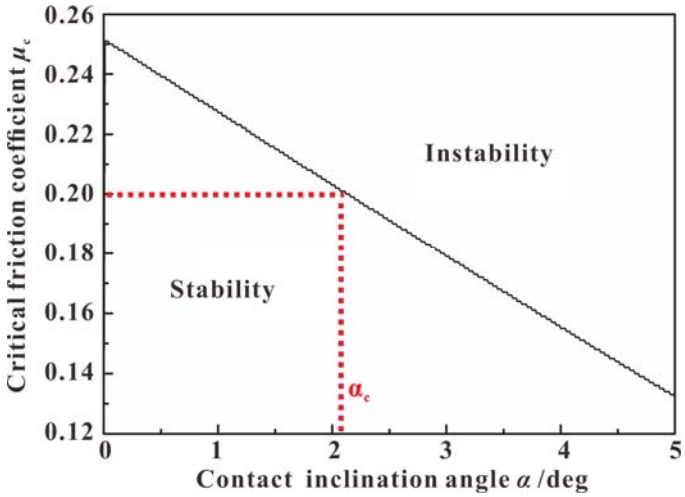

Fig. 21 Relationship between the contact inclination angle α and critical friction coefficient μ

Fig. 22 presents a relationship between the dynamic response and the tribological characteristics of the damped and undamped components friction systems. For the Original friction

system, the larger contact inclination angle during the sliding process causes severe the tangential partial wear, which triggers the instability of the friction system and consequently results in large vibration amplitude. Meanwhile, introducing the slotted-structured damping components into the system can significantly reduce the contact inclination angle, thus alleviating the partial wear of the contact interface and stabilizing the friction system. It is a common sense [36] that the contact stress distribution at the friction interface is a key factor influencing the friction-induced vibration of the friction system. The inclination angle is an index that can reflect the contact status, if the angel is small, the effective interfacial contact area is large, and vice versa. A large contact inclination angle can lead to contact stress concentration at the leading edge of the friction pad. Generally, the contact stress concentration at the leading edge of the friction pad will lead to tangential partial wear, which consequently aggravates the wear situation of the friction interface and results in poor vibration performance. Therefore, a small contact inclination angle contributes to stabilizing the friction system and vice versa.

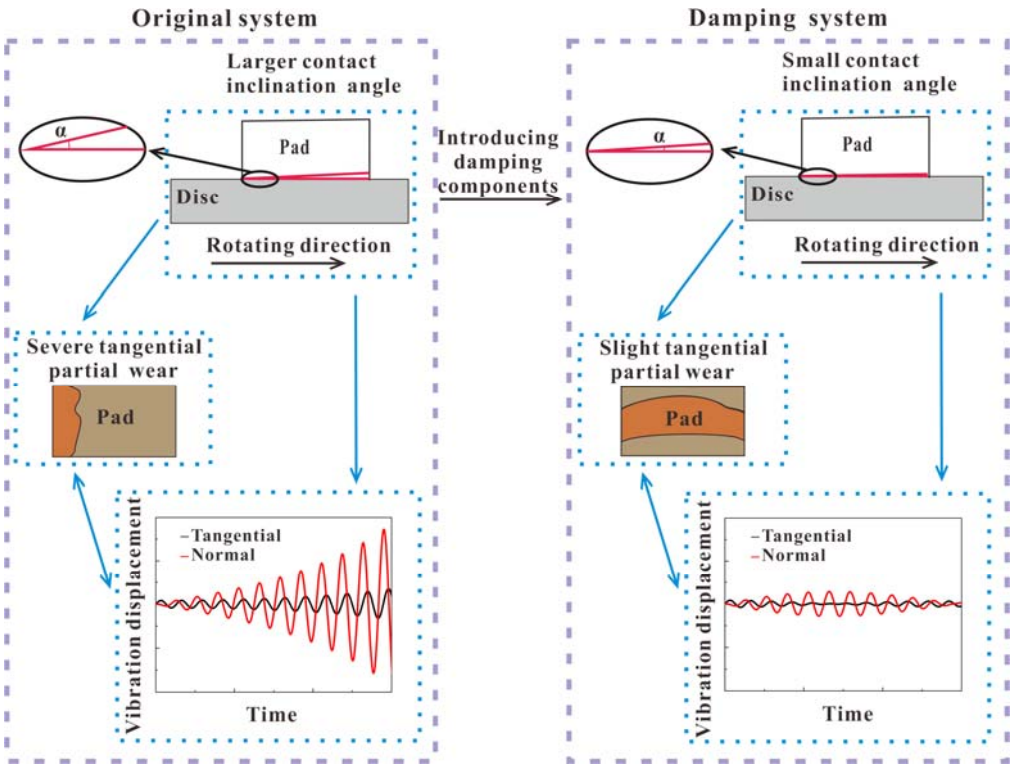

Fig. 22 Mechanism of the effects of damping components on the tribological and dynamic response characteristics of friction systems

4. Conclusions

In this study, the effect of the damping components having slots at different-depths on the instability of the system is evaluated using a special tribological test apparatus. Experimental tests and numerical simulations are performed to reveal the mechanism underlying the effect of the damping components on the vibration response characteristics of the systems. The main conclusions drawn are presented as follows:

(1) The experimental results show that the damping components with slotted surface structures can reduce the vibration response of the systems and the energy level at the dominant frequency, thus stabilizing the systems. Specifically, the damping components having slots of specific depths show the highest potential in suppressing the instability. Moreover, When the normal force fluctuates normally in the process of friction sliding, the stability degree of the friction system can be reflected from the friction coefficient. The more stable the system is, the less the friction coefficient fluctuates.

(2) Tangential partial wear on the pad surface can reflect the matching degree of contact interface of the friction pairs and the vibration characteristics of the systems. The damping components with slotted surface structures can mitigate the tangential partial wear and improve the matching degree of contact interface of the friction pairs, which can further effectively reduce the instability of the system induced by friction sliding. Therefore, eliminating the tangential partial wear of the pad surface can effectively reduce the instability of the system induced by friction sliding.

(3) The numerical results indicate that the contact inclination angle between the friction pair can significantly affect the instability of the systems. Introducing the slotted damping components with the friction system can reduce the contact inclination angle, consequently alleviating the severe tangential partial wear at the contact interface and suppressing the instability of the systems.

Acknowledgements

The authors are grateful for the financial support of the National Natural Science Foundation of China (Nos. 51822508 and 11672052), the opening project support of the Key Laboratory of Testing Technology for Manufacturing Process (Southwest University of Science and Technology), Ministry of Education (No. 18kfzk01), and Sichuan Province Science and Technology Support Program (No. 2020JDTD0012).

References

[1] Kang, Jaeyoung. Theoretical Model for Friction-Induced Vibration of Ball Joint System under Mode-Coupling Instability. Tribology Transactions, 2015, 58(5):00-00.

[2] Liu N, Ouyang H. Suppression of friction-induced-vibration in MDoF systems using tangential harmonic excitation. Meccanica, 2020.

[3] Cui X, Cheng Z, Yang Z, et al. Study on the phenomenon of rail corrugation on high-speed rail based on the friction-induced vibration and feedback vibration. Tribology Transactions, 2020

[4] Angulo F, Olivar G, Osorio G A, et al. Bifurcations of non-smooth systems. Communications in Nonlinear ence & Numerical Simulation, 2012, 17(12):4683-4689.

[5] Boris Ryzhik. Suppression of Friction-Induced Bending Vibrations in a Flexible Disk Sliding in Contact With a Rigid Surface. Journal of Vibration and Acoustics, 2014.

[6] Cornelius, Weiss, Michael. Friction induced dynamics of ball joints: Instability and post bifurcation behavior. European Journal of Mechanics A solids, 2014.

[7] Meziane A, Baillet L, Laulagnet B. Experimental and numerical investigation of friction-induced vibration of a beam-on-beam in contact with friction. Applied Acoustics. 2010;71:843-53.

[8] Hoffmann NP, Gaul L. Friction induced vibrations of brakes: Research fields and activities. Sae Technical Papers. 2008, 16:145-60.

[9] Jung S P, Song H S, Park T W, et al. Numerical Analysis of Thermoelastic Instability in Disc Brake System. Applied Mechanics & Materials, 2012, 110-116:2780-2785.

[10] Meehan P A. Prediction of wheel squeal noise under mode coupling. Journal of Sound and Vibration, 2019, 465:115025.

[11] Lu C, Martínez-Esnaola JM. Multiaxial fatigue space: A three-dimensional space constituted of fatigue basic units, International Journal of Fatigue. 2020 doi: https://doi.org/10.1016/j.ijfatigue.2020, 105995.

[12] Renault A, Massa F, Lallemand B, Tison T. Experimental investigations for uncertainty quantification in brake squeal analysis. Journal of Sound and Vibration. 2016, 367:37-55.

[13] Oberst S, Lai J, Marburg S. Guidelines for numerical vibration and acoustic analysis of disc brake squeal using simple models of brake systems. Journal of Sound and Vibration. 2013, 332:2284-99.

[14] Zhang L, Wei C, Hu J, et al. Nonlinear Dynamic Characteristics of Rub-Impact Process at High Circumferential Velocities in No-Load Multiplate Wet Clutch. Tribology Transactions, 2019.

[15] Ngoya E, Almudena Suárez, Sommet R, et al. Steady state analysis of free or forced oscillators by harmonic balance and stability investigation of periodic and quasiperiodic regimes. International Journal of RF and Microwave Computer-Aided Engineering, 2010, 5(3):210-223.

[16] Abdo J A . Investigation of Contact Stiffness and its Relation to Friction-Induced Noise and Vibration. International Journal of Modelling and Simulation, 2015, 26(4):295-302.

[17] Neis PD, Ferreira NF, Fekete G, Matozo LT, Masotti D. Towards a better understanding of the structures existing on the surface of brake pads. Tribology International. 2017, 105:135-47.

[18] Graf M, Ostermeyer G-P. Instabilities in the sliding of continua with surface inertias: an initiation mechanism for brake noise. Journal of Sound and Vibration. 2011, 330:5269-79.

[19] Singh R. Motion and Vibration Control Using Passive and Active Hydraulic Mounts: Improved Nonlinear and Quasi-Linear Models, Latest Design Trends and Some Insights.

[20] Hasegawa K, Satoh Y. Dynamic properties of filled rubber for small oscillation. The Proceedings of the Dynamics & Design Conference, 2010, 76(765):1295-1300.

[21] Lu X D, Zhao J, Mo J L, et al. Suppression of Friction-Induced Stick－Slip Behavior and

Improvement of Tribological Characteristics of Sliding Systems by Introducing Damping Materials[J]. Tribology Transactions, 2019, 63(1):1-16.

[22] Ouyang H, Wang D W, Zhou Z R, et al. Disc surface modifications for enhanced performance against friction noise. Applied Surface Science: A Journal Devoted to the Properties of Interfaces in Relation to the Synthesis and Behaviour of Materials, 2016.

[23] Wang D W, Mo J L, Liu M Q, et al. Noise performance improvements and tribological consequences of a pad-on-disc system through groove-textured disc surface. Tribology International, 2016, 102:222-236.

[24] Lin SC, Bakar ARA, Harujan WMMW, Ghani BA, Jamaluddin MR. Suppressing disc brake squeal through structural modifications. Jurnal Mekanikal. 2009, 29.

[25] Oberst S, Lai J. Numerical prediction of brake squeal propensity using acoustic power calculation. Proceedings of ACOUSTICS 2009. 2009.

[26] Kim SJ, Jang H. Friction and wear of friction materials containing two different phenolic resins reinforced with aramid pulp. Tribology international. 2000, 33:477-84.

[27] Gweon JH, Joo BS, Jang H. The effect of short glass fiber dispersion on the friction and vibration of brake friction materials. Wear. 2016, 362-363:61-7.

[28] Ahmed I, Metwally S, Mohamed E, Abouel-Seoud S. Influence of surface modifications on vehicle disc brake squeal. SAE Technical Paper. 2009.

[29] Baik S H. High damping Fe–Mn martensitic alloys for engineering applications. Nuclear Engineering & Design, 2000, 198(3):241-252.

[30] Fritz G, Sinou J-J, Duffal J-M, Jézéquel L. Investigation of the relationship between damping and mode-coupling patterns in case of brake squeal. Journal of Sound and Vibration. 2007, 307:591-609.

[31] Nakra B. Vibration control in machines and structures using viscoelastic damping. Journal of sound and vibration. 1998, 211:449-66.

[32] Triches Jr M, Gerges S, Jordan R. Reduction of squeal noise from disc brake systems using constrained layer damping. Journal of the Brazilian Society of Mechanical Sciences and Engineering. 2004, 26:340-8.

[33] Wang X C, Mo J L, Ouyang H, et al. Squeal Noise of Friction Material With Groove-Textured Surface: An Experimental and Numerical Analysis. Journal of Tribology, 2016, 138(2):021401.

[34] Kang J. Finite element modelling for the investigation of in-plane modes and damping shims in disc brake squeal. Journal of Sound and Vibration. 2012, 331:2190-202.

[35] Zhang Q, Mo J, Lu X, Zhao J, Wang D, Zhou Z. Grooved-structure design for improved component damping ability. Tribology International. 2018, 123:50-60.

[36] Lu X D, Zhao J, Mo J L, et al. Improvement of dynamical and tribological properties of friction systems by introducing parallel-grooved structures in elastic damping components. Composite Structures, 2018, 192:8-19.

[37] John E. Mottershead, Maryam G. Tehrani, Yitshak M. Ram. Eigenvalue Assignment Problems in Vibration Using Measured Receptances: Passive Modification and Active Control Dynamical Inverse Problems: Theory and Application. Springer Vienna, 2011.

[38] Chen G X, Zhou Z G, Kapsa P, Vincent L. Effect of surface topography on formation of squeal under reciprocating sliding. Wear. 2002, 253:411-23.

[39] Tomota T, Kondoh Y, Ohmori T. Modeling Solid Contact between Smooth and Rough

Surfaces with Non-Gaussian Distributions. Tribology Transactions, 2019, 1-21.

[40] Hoffmann N, Fischer M, Allgaier R, Gaul L. A minimal model for studying properties of the mode-coupling type instability in friction induced oscillations. Mechanics Research Communications. 2002, 29:197-205.

[41] Hoffmann N, Gaul L. Effects of damping on mode‐coupling instability in friction induced oscillations. Journal of Applied Mathematics & Mechanics, 2003, 83(8).